Xue, Q., Wang, Z., and Chen, Q. 2021. "Multi-objective optimization of building design for life cycle cost and CO2 emissions: A case study of a low-energy residential building in a severe cold climate," *Building Simulation*, DOI: 10.1007/s12273-021-0796-5.

Multi-objective optimization of building design for life cycle cost and CO_2 emissions: A case study of a low-energy residential building in a severe cold climate

Qingwen Xue[1, 2, 3], Zhaojun Wang[1, 3, *], Qingyan Chen[2]
[1]School of Architecture, Harbin Institute of Technology, Harbin, 150090, China
[2]School of Mechanical Engineering, Purdue University, West Lafayette, IN 47907, USA
[3]Key Laboratory of Cold Region Urban and Rural Human Settlement Environment Science and Technology, Ministry of Industry and Information Technology, Harbin, 150090, China
[*]*Corresponding email: wangzhaojun@hit.edu.cn*

Abstract

Currently, building construction and operation are responsible for 36% of global final energy usage and nearly 40% of energy-related carbon dioxide (CO_2) emissions. From the sustainable development perspective, it is crucial to consider the impact of construction material on the achievement of life cycle benefits. This study proposed a simulation-based multi-objective optimization method to minimize both life cycle cost and CO_2 emissions of buildings. We built an energy simulation model with hybrid ventilation and light-dimming control in EnergyPlus based on an operational passive residential building in a severe cold climate. Next, this investigation selected insulation thickness, window type, window-to-wall ratio, overhang depth and building orientation as design variables. The study ran parametric simulations to establish a database and then used artificial neural network models to correlate the design variables and the objective functions. Finally, we used the multi-objective optimization algorithm NSGA-II to search for the optimal design solutions. The results showed potential reductions of 10.9–18.9% in life cycle cost and 13.5–22.4% in life cycle CO_2 emissions compared with the initial design. The results indicated that the optimization approach in this study would improve building performance. The optimal values of the design variables obtained in this study can guide designers in meeting economic and environmental targets in passive buildings.

Keywords: Passive building; Artificial neural network; Life cycle CO_2 emissions; Natural ventilation; Multi-criteria optimization

1. Introduction

Currently, building construction and operation are responsible for 36% of global final energy usage and nearly 40% of energy-related CO_2 emissions (Global ABC 2020). This energy use will potentially grow by more than 50% by 2050 without energy-efficiency improvements in the building sector (Guo et al. 2021). In response to these issues, building energy efficiency regulations have been developed worldwide to reduce energy consumption and mitigate environmental problems. Among the many building design guidelines, the concept of a net zero energy building (nZEB), namely, the "passive house", originated in Europe and has attracted increasing attention around the world. The nZEB guidelines have been adapted for the local climates of various countries. Recently, China issued a

"Technical standard for nearly zero energy buildings" to guide building design for its five climate zones (MOHURD 2019). According to report by building energy research center in China, heating accounts for more than 65% of the total energy consumption in buildings in northern China, and up to 90% in severe cold areas (Building Energy Research Center 2016). Therefore, in these regions, the current trend is to use passive interventions such as thick insulation and high-performance windows to reduce heat losses through the envelope.

However, there are two existing problems with regard to the building envelope design. First, in heating-dominated regions, the energy-efficient measures minimize the heating demand of buildings by using thick insulation and high airtightness, but these measures increase the discomfort hours in summer without cooling systems. Thus, many previous studies (Baba and Ge 2020; Guo et al. 2020; Wang et al. 2020) reported too-high temperatures inside these buildings in summer. If the buildings used cooling systems, the annual energy cost would be high because cooling requires electricity, which is three times more expensive than the fossil fuel used for heating. Second, the initial costs of these energy-efficient measures are so high that the payback time is many years long. According to (Yang et al. 2019), the construction cost for a residential nZEB is 722 CNY/m^2 higher than that for a conventional building on average. This expense prevents massive implementation of nZEBs, despite their energy efficiency.

Fig. 1 (Boermans et al. 2011) displays a cost curve for an nZEB. This curve represents life cycle cost (LCC) as a function of primary energy consumption, which has a minimum value for the cost-optimal solution. The right side of the curve represents poor performance in terms of both energy and cost. The left side of the curve characterizes nZEBs, which have very low energy requirements but entail high initial and global costs. It is generally understood that the greater initial costs should be returned by the reduced energy bills over the lifespan of a building. Otherwise, the design solution would not be economically feasible. In addition to the initial investment, interventions such as thicker insulation or higher-performance windows would have an environmental impact, derived from the manufacture, installation, dismantling and disposal of the materials (Sartori and Hestnes 2007; Cabeza et al. 2013; Dylewski and Adamczyk 2016). Neglecting such an impact might lead to solutions by which operational energy savings are attained at the expense of increased environmental burdens elsewhere (Carreras et al. 2016, 2017). Therefore, it is crucial to investigate the building life cycle benefits.

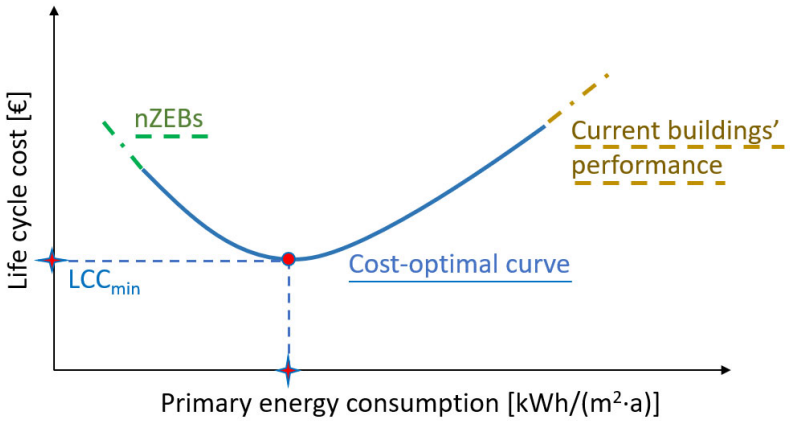

Fig. 1. Cost-optimal curve for building energy design (Boermans et al. 2011)

An optimization problem for a passive building is the maximization of the main sustainable benefits in terms of economic and environmental aspects (Jafari and Valentin 2018). For the purpose of sustainability, a life cycle assessment (LCA) considering all phases, including pre-use, use, and end-of-life, has been widely employed to quantify economic and environmental impacts (BS EN 2011). In terms of economic benefits, LCC analysis is frequently used to compare the initial investments and future benefits of passive design alternatives for building energy efficiency. Similar to LCC, life cycle environmental impact combines materials (embodied building impacts) and building use (i.e., energy consumption), as indicated by global warming potential (CO_2 equivalent mass), acidification potential (SO_2 equivalent mass), particulates that affect human health (PM2.5 equivalent mass), eutrophication potential (N equivalent mass), smog potential (O_3 equivalent mass), ozone depletion potential (CFC 11 equivalent), etc. (ISO 2017). CO2 is the most commonly used indicator of the environmental impact of buildings, in response to the imminent threat of global warming.

Previous studies investigated building envelope design by means of LCA approach. Mateus et al. (2019) compared four energy renovation scenarios regarding the LCC and environmental performance. A similar work explored the potential of LCC for green building strategies by conducting energy simulations for different energy conservation measures (Hajare and Elwakil 2020). The results indicated a 13.5 % reduction in the building cost when a combination of passive design and active strategies was employed. Such studies have assessed the use of LCA in a variety of scenarios to improve building performance, but not to identify the optimal solution. Other studies have addressed the optimization of the building envelope design, but mostly with a focus on individual design parameters. For example, Marino et al. (2017) conducted a parametric analysis to optimize window-to-wall ratios (WWRs). Alsayed and Tayeh (2019) investigated the economic benefits of insulation thickness with two different materials. These studies focused on “local design optimization”. However, actual building design includes many variables such as building orientation, thermal insulation, window glazing, and window size and shading, which interact with each other in the construction of variable space (Ferrara et al. 2018). Designers should take into account the best combination of these parameters as a whole. It is essential to adopt a “global design optimization” approach combining chosen variables that can be interactively evaluated. For a specific aim expressed as objective functions under several constraints, one can search for the globally optimal solutions among the possible options. For example, Bichiou and Krarti (2011) performed a global optimization to determine the building design features that minimize the life cycle costs and found that the optimal selections can reduce life cycle costs by 10–25%.

Nowadays, an increasing number of objectives are considered in the design of a passive building, such as energy saving, indoor environment quality, cost minimization and reduction of environmental impacts, and this reality calls for multi-objective optimization of design solutions. It is important to conduct multi-criteria analyses in the architect’s design process, especially in early design phases when the possibility of modifying the design is usually high (Płoszaj-Mazurek et al. 2020). Kiss and Szalay (2020) conducted an environmental multi-objective optimization on building to provide design options with the lowest environmental impact for the whole life cycle. The various building performance

indicators are often competing with each other. To solve multi-objective optimization problems, several studies have implemented algorithms such as particle swarm optimization (PSO), the artificial bee colony (ABC), and the non-dominated sorting genetic algorithm II (NSGA-II). For example, Lu et al. (2017) employed PSO to reduce the energy consumption with consideration of envelope parameters, shading system, and a courtyard. Delgarm et al. (2016) utilized an ABC algorithm to obtain the optimal solutions for the comfort-energy efficient configurations of a building envelope. Zhai et al. (2019) used NSGA-II to obtain the optimal window parameters for energy consumption, indoor thermal environment and visual performance, simultaneously. Among these algorithms, NSGA-II has been more widely used in the field of architecture for efficient handling of non-linear problems (Machairas et al. 2014) and is promising in the identification of the optimum solutions to complex problems (Garshasbi et al. 2016).

Based on the literature review above, two research gaps were identified. First, LCAs for passive buildings in severe cold regions of China are seldom studied. Buildings with very high energy performance have become technically feasible in China, and the main difficulties lie in improving the economic and environmental performance of nZEBs. Second, natural ventilation (NV) is prevalent in summer and can greatly reduce cooling energy usage (Spentzou et al. 2018; Ameur et al. 2020). However, the optimal building design parameters under hybrid ventilation (HV) conditions, combining NV and air-conditioning, have not yet been investigated. The present study attempts to fill these gaps.

Therefore, this study aimed to simultaneously minimize cost and CO_2 emissions over the life cycle of a building by simulation-based multi-objective optimization. The simulation model contains the designed HV and light-dimming control strategies. The optimization results were intended to provide quantitative solutions that would assist decision-making in nZEB design, for the achievement of economic and environmental targets.

2. Methods

To optimize a building design, we first selected a reference passive building and simulated its energy use in EnergyPlus. Next, we defined the objective functions and design variables with determined distributions. We then conducted parametric simulations to establish a database of the relationship between the design variables and objective functions. We modelled the complex relationship with the use of artificial neural network (ANN) models. Finally, we conducted multi-objective optimization to search for the optimal design solutions.

2.1 Modelling of the reference building

2.1.1 Description of climate and building features

A passive residential building located in Harbin was selected as the reference building. Harbin (45°41′N 126°37′E) is a typical city in the severe cold zone of China, where the outdoor temperature is extremely low in winter, ranging from −25 °C to −5 °C. In this region, centralized district heating systems are widely used, with an operating period of nearly half a year, from mid-October to mid-April of the following year. Meanwhile, the outdoor temperature is relatively cool in summer, and the cooling operating period is only from early June to late August.

The reference building was a typical high-rise building with 11 stories. Fig. 2 shows the appearance of the building and the floor plan of a standard unit. The building had an overall usable floor area of around 8580 m^2, with 66 apartments in total. The floor area of each household was about 80-90 m^2, and the height was 2.78 m. A typical household consisted of a living room with a dining room, two bedrooms, a bathroom and a kitchen. The orientation of the building was 45° north by west.

(a) (b)

Fig. 2. (a) Photograph of the building and (b) floor plan of a unit

In the severe cold region, residential buildings must meet stringent requirements for insulation and airtightness. The passive building in this study was very well-insulated, with 300 mm expanded polystyrene (EPS) on the exterior walls and the roof. The windows used triple-glazed, low-e glass with argon filling the air layers; the thermal transmittance (U-value) was 0.8 W/m^2 K, and the solar heat gain coefficient (SHGC) was 0.65. The WWRs on the east, west, north, and south were 5.71%, 4.16%, 28.53%, and 33.93%, respectively. Further details of the building envelope are provided in Table 1.

Table 1 Structural and material properties of the building envelope

Construction component	Layers (from exterior to interior)	Thickness (mm)	Conductivity (W/m·K)	Density (kg/m^3)	Specific heat (J/kg·K)
Roof	Fine aggregate concrete	40	1.74	2500	920
	Waterproof layer	--	--	--	--
	Cement mortar	20	0.93	1800	1050
	EPS	300	0.033	20	1647
	Cement mortar	20	0.93	1800	1050
	Reinforced concrete	120	1.74	2500	920
	Mixed mortar	20	0.87	1800	1050
Exterior wall	EPS	300	0.033	20	1647
	Ceramsite block	200	0.49	76	600
	Mixed mortar	20	0.87	1800	1050
Exterior window	Low-e clear float glass	3	0.99	2528	880
	Argon cavity	13	0.0177	1.784	520
	Clear float glass	3	0.99	2528	880
	Air cavity	13	0.026	1.225	1010

	Low-e clear float glass	3	0.99	2528	880

This study used EnergyPlus (v. 9.2.0) to perform the energy simulation, and SketchUp to construct the building geometry model. To conduct an energy simulation, we needed to set values for various thermophysical properties in EnergyPlus: building envelope parameters, internal heat gains, shading overhang system, lighting control system, and heating, ventilation and air conditioning (HVAC) system. The building envelope parameters were set to the values listed in Table 1. As for the internal heat gains, Table 2 specifies the heat gains of the occupants, equipment, and lighting and the corresponding usage schedules. Although shading overhangs were not present on the reference building, we considered the use of overhangs in the following parametric simulation. The shading position was above the window, and the left and right extensions of each overhang were fixed at zero. The depth of the overhang was one of the design parameters to be optimized. For west-facing windows, vertical fins were adopted, whereas no external shading device was assumed to be present outside the north and east windows. As for the HVAC system, this study used "IdealLoadsAirSystem" in EnergyPlus; the setpoint temperatures were 26 °C in summer and 20 °C in winter.

Table 2 Internal heat gains

Source of internal heat gain	Heat gain	Schedule	
		Weekday	Weekend
Occupant	100 W/occupant	00:00–8:00 and 18:00–24:00	Always at home
Refrigerator	150 W	Always on	
Lighting	6 W/m^2	See Section 2.1.3	
Television	60 W	18:00–22:00	8:00–10:00 and 18:00–23:00

2.1.2 Hybrid ventilation control

In general, free energy sources, such as natural ventilation and daylight, should be taken into full consideration in the design of zero/low-energy buildings in order to satisfy the requirement of minimal energy consumption. Therefore, we proposed a hybrid ventilation strategy for control of NV and a light-dimming strategy for control of electric lighting. The detailed control logic for HV consisting of NV and air conditioning is described in Section 2.1.2, and the lighting control is introduced in Section 2.1.3.

Control of HV was proposed in this study to maximize the benefits of passive design strategies. In heating-dominated regions, the effects of thick insulation and high airtightness on energy conservation are more pronounced. However, the insulation and airtightness also increase the use of cooling energy (Li et al. 2013). When the outdoor temperature is cool in the shoulder and summer seasons, NV can be used effectively to improve human thermal comfort and reduce the building cooling demands. Therefore, we built such a control logic for the hybrid ventilation. In those cases in which NV did not provide sufficient cooling, and overheating occurred, the windows were closed and the cooling system was turned on.

We integrated an HVAC system with NV by programming the "hybrid ventilation availability manager" in the Energy Management System of EnergyPlus. Our controller had two purposes: 1) to prevent simultaneous NV and HVAC system operation, and 2) to reduce the space cooling load by NV. The NV

modeling was performed with the use of the AirFlowNetwork (AFN) in the EnergyPlus program, which applies the AIRNET algorithm. The object AirflowNetwork:MultiZone:Component:DetailedOpening specifies the properties of air flow through windows and doors when they are closed or open. For the naturally ventilated state, ASHRAE Standard 55 (ASHRAE 2017) sets the range of comfortable indoor operative temperature within the upper and lower 80%/90% adaptive comfort acceptability limits. An acceptability of 90% was adopted in this study. To assess whether it was favorable for the use of NV, an indoor operative temperature was calculated and compared with the 90% acceptability upper limits of the ASHRAE Standard 55 adaptive comfort model. A single cooling setpoint controller was used as the HVAC system thermostat in order to comply with the upper limit of the adaptive comfort model. This limit varies from month to month with the prevailing outdoor air temperature (de Dear and Brager 2002). Fig. 3 shows the adaptive comfort range and the 90% acceptability upper limits for June, July, and August, which were calculated as 26.73 °C, 27.88 °C, and 26.84 °C, respectively.

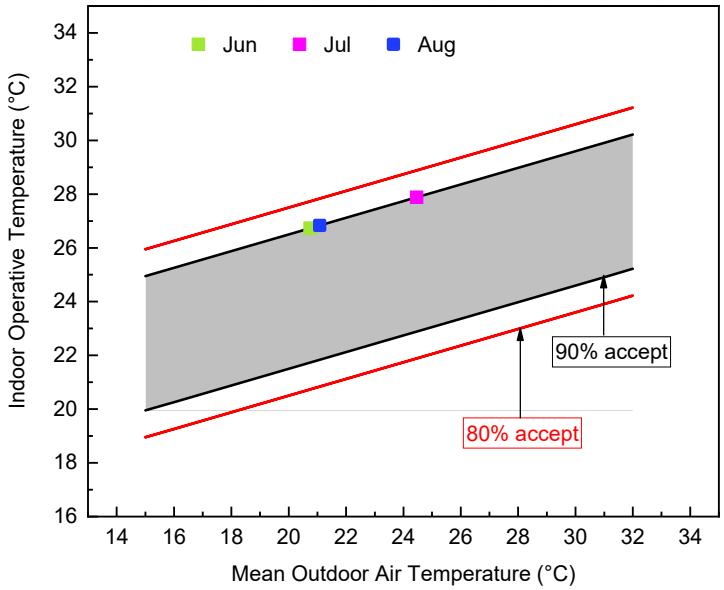

Fig. 3 Monthly cooling temperature setpoints according to the ASHRAE 55 adaptive comfort model, applicable to the naturally ventilated state.

Fig. 4 illustrates the control logic. The controller can override local controls for both HVAC and AFN. The NV usage depends on the following parameters: room occupancy, outdoor air temperature, indoor operative temperature, and air temperature in the thermal zone. If the outdoor air temperature is within the preset upper and lower limits, then NV is possible. Next, the indoor operative temperature is calculated. If it can be controlled within the comfortable zone and if the outdoor temperature is lower than the indoor temperature at the same time, then NV is used and no cooling is needed. Otherwise, NV is not sufficient to ensure thermal comfort, and HVAC system operation is allowed if the current time is within the system's operating hours. Since window area would affect NV, the cooling energy consumption could be determined under different configurations of windows size and building orientation.

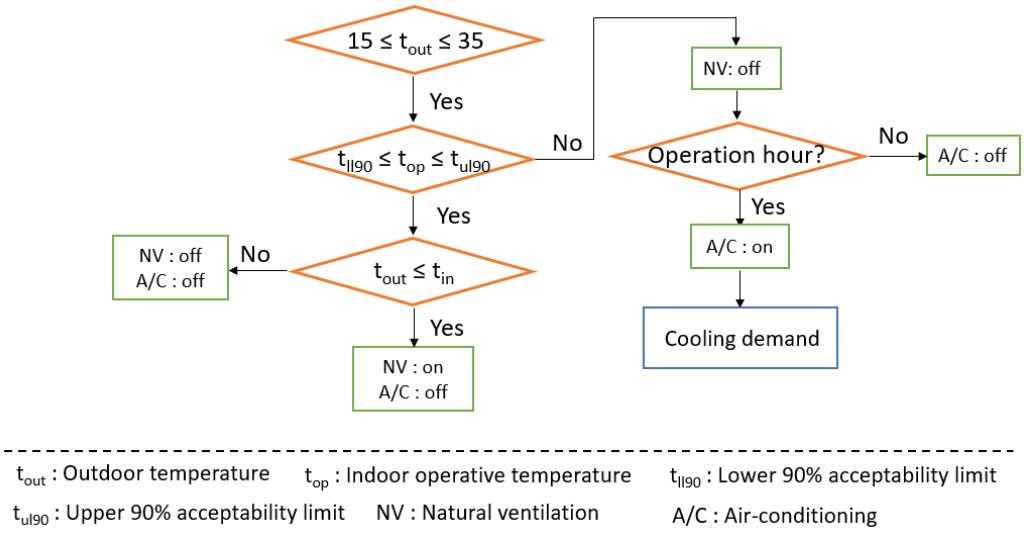

Fig. 4 Hybrid control logic for NV and air-conditioning operation during the cooling season in the simulation.

2.1.3 Light-dimming control

The lighting illuminance level for the residential buildings in this study was based on Chinese code GB50034-2013. Illuminance levels above 100 lx for bathrooms, 150 lx for bedrooms, kitchens, and dining rooms, and 300 lx for living rooms meet the indoor lighting requirements. In this study, the reference points were the center of each room at a height of 0.75 m.

A simplified daylight control model, "continuous/off dimming control," was applied for artificial lighting. The model has a daylight-sensing controller that switches the lighting on or off automatically according to the illuminance set-point. For each simulation, the daylight illuminance level at the specified indoor reference point was first calculated. When the minimum dimming point was reached, the lights were switched off completely. When the calculated indoor illuminance was below the set-point, artificial lighting was turned as a supplement, in accordance with the schedule of occupant presence in the unit. A lighting density of 6 W/m^2 was implemented in those cases in which the minimum dimming point could not be reached. The illuminance set-points for each room and the lighting density are shown in Table 3.

Table 3 Illuminance set-points and artificial lighting density.

Type of room	Illuminance level (lx)	Artificial lighting density (W/m^2)
Living room	300	6
Bedroom	150	
Dining room	150	
Kitchen	150	
Bathroom	100	

Daylight illuminance can be affected not only by sky conditions and sun position, but also by the transmittance of window glass and by window-shading devices. Therefore, lighting energy

consumption can be determined under different configurations of the windows and shading system.

2.2 Objective functions and design variables

2.2.1 Determination of design variables and constraints

The selected variables are design parameters of building components. They are on the one hand reducing energy demand, while on the other hand increasing investment cost. The maximum point of feasibility refers to the economic point beyond which further investment cannot be returned in energy savings over the building life cycle. Beyond this point, the emphasis will be on the added environmental benefits.

For severe cold climates, the heat transfer coefficients of external walls and windows, shading, SHGC of windows, and WWRs are the main factors in building energy consumption (Thalfeldt et al. 2013; Zhao et al. 2015). Window type in relation to the heat transfer coefficient and SHGC of the window should be treated as a single variable, so that the cost and CO_2 emissions can be described quantitatively. In addition, building orientation is usually essential for window and shading design. We ultimately selected nine parameters for the optimization problem, including the building orientation, wall insulation thickness, roof insulation thickness, external window type, WWRs for the south, north, east and west faces, and south shading overhang depth.

All the parameters were continuous except the window type, which can only take on integer values. We evaluated all the related components quantitatively in terms of cost and CO_2 emissions. For determination of the ranges of the selected design variables, the variables were divided into three categories. First, for the parameters that are clearly defined in the passive building (PB) standard, such as the U-value of envelope components and the SHGC, the upper and lower limits of the ranges were typically based on the conventional building (CB) standard (MOHURD 2010) and PB standard (MOHURD 2019), respectively, for the severe cold region. The U-value of envelope components could be changed by adjusting the insulation thickness. Second, WWRs for different orientations were determined in accordance with the CB standard. Third, for those parameters that are not be clearly defined by norms or standards, the ranges were determined according to the relevant literature (Zhai et al. 2019). The continuous variables had uniform distributions over their preset ranges. For window type, which was treated as a discrete quantity, six different types were investigated. The costs of the components were estimated from market surveys. Table 4 lists the design variables and their ranges of variation.

Table 4 Design variables and ranges of variation

Variable	Range and interval	Performance	Cost
Wall insulation thickness (mm)	[50: 20: 300]	K = 0.1~0.7 W/(m^2·K)	600 CNY/m^3
Roof insulation thickness (mm)	[110: 20: 330]	K = 0.08~0.45 W/(m^2·K)	600 CNY/m^3
External window type	Type 1: Double pane	K = 2.5 W/(m^2·K), SHGC = 0.7	890 CNY/m^2
	Type 2: Double pane, low-e	K = 2 W/(m^2·K), SHGC = 0.6	920 CNY/m^2
	Type 3: Double pane, low-e, argon	K = 1.5 W/(m^2·K), SHGC = 0.6	1200 CNY/m^2

	Type 4: Triple pane, low-e	K = 1.2 W/(m^2·K), SHGC = 0.55	1900 CNY/m^2
	Type 5: Triple pane, low-e (green)	K = 1.0 W/(m^2·K), SHGC = 0.5	2300 CNY/m^2
	Type 6: Triple pane, low-e, argon	K = 0.8 W/(m^2·K), SHGC = 0.45	2600 CNY/m^2
South WWR (%)	[5: 5: 45]	--	--
North WWR (%)	[5: 5: 25]	--	--
West/East WWR (%)	[5: 5: 30]	--	--
Overhang depth (m)	[0: 0.2: 1.5]	--	300 CNY/m^2
Orientation (°)	[0: 15: 90] & [270: 15: 360]	--	--

2.2.2 Objective functions

Life cycle CO_2 ($LCCO_2$) emissions and LCC were selected as the objective functions in this study. The optimization problem was to minimize LCC and $LCCO_2$ by adjusting the design parameters, expressed as Min{$F_1(\mathbf{x})$=LCC, $F_2(\mathbf{x})$=$LCCO_2$}, $\mathbf{x} = [x_1, x_2, \ldots, x_n]$.

The LCC is the sum of the present values of investment and operating costs over the building lifecycle. A 30-year period was considered for the life cycle analysis (EU Commission 2012). The lifespans of insulation material, windows and shading devices are generally 30 years or longer; therefore, replacement costs were not taken into account in this study. As for the investment cost, since the main structure was the same in all cases and did not affect the cost result, only the extra investment costs that arose from changes in design variables were involved in the calculation. On the basis of standard EN 15459-1 (BS EN 2017), LCC was calculated by the following formula:

$$LCC = dIC + \sum_{i=0}^{n} a(r_e, i) \bullet EC \quad (1)$$

where:

- dIC—the differences in investment cost between the reference and optimized building cases, CNY;
- a—present value factor which depends on the real interest rate r_e (market interest rate adjusted for inflation in energy price) and on the timing of the costs i (number of years after the starting year);
- n—the number of years under investigation, 30 in this study;
- EC—annual energy costs, CNY.

The annual energy cost for the year i represents the sum of heating, cooling and lighting energy consumption in that year. It was calculated by the following formula:

$$EC = \frac{Q_H}{H \cdot \eta_H} \bullet P_H + (\frac{Q_C}{\eta_C} + E_L) \bullet P_E \quad (2)$$

where:

- Q_H—annual heating demand, kWh/(m^2·a);
- H—conversion factor of heating energy to coal consumption, kg/kWh;
- η_H—annual efficiency of heating system, η_H = 0.92;
- P_H—price of energy from coal, CNY/kg;
- Q_C—annual cooling demand, kWh/(m^2·a);

- η_c—annual efficiency of cooling system, η_c = 3;
- E_L—annual lighting energy consumption, kWh/(m^2·a);
- P_E—price of energy from electricity, CNY/kWh.

To make a reasonable comparison among the costs occurring at different times, these costs must be adjusted for changes in purchasing power. The present value factor adjusts the future costs of annual energy to the present value, to make them comparable with the initial investment at the time of installation. This factor depends on the interest rate r_e (market interest rate adjusted for inflation) and the timing of the costs (number of years after the starting year), calculated by the following formulas:

$$a = \frac{1-(1+r_e)^{-i}}{r_e} \tag{3}$$

$$r_e = \frac{r-e}{1+e} \tag{4}$$

$$r = \frac{r_i - f}{1+f} \tag{5}$$

where:

- r_e—market interest rate including the effect of energy price escalation, %;
- i—number of years;
- r—real interest rate, %;
- e—escalation of energy prices over the inflation rate in the analyzed period, 1.2%;
- r_i—nominal rate, 7%;
- f—inflation rate, 2%.

The second objective was to minimize CO_2 emissions over the life cycle of the building. It was necessary to apply a carbon emission factor (CEF) in order to calculate the corresponding carbon emissions of construction materials and energy consumed. CEF is a coefficient that represents the quantity of CO_2 and its equivalents emitted from one unit of a certain type of material or fuel. The determination of CEF is based on the CLCD database in China. The CEFs used in this study are summarized in table 6.

Table 6 Carbon emission factors (CEFs) for different kind of materials and fuels

Material /fuel	EPS (kg/kg)	Window (kg/m^2)	Overhang (kg/m^2)	Coal (kg/kg)	Electricity (kg/kWh)
CEF	5.02	122.5	227.34	2.27	1.15

The CO_2 emission of a building can be expressed as:

$$LCCO_2 = \sum_{j=1}^{J} Q_j \times f_j + n \times \left[\frac{Q_H}{H \cdot \eta_H} \bullet f_{coal} + \left(\frac{Q_C}{\eta_C} + E_L\right) \bullet f_{ele} \right] \tag{6}$$

where:

- J—type of construction material;
- Q_j—quantity of the specific material;

- f_j—CEF of the specific material, kg/material;
- f_{coal}—CEF for coal, kg/kg;
- f_{ele}—CEF for electricity, kg/kWh.

2.3 Optimization procedure

2.3.1 Parametric simulations

Following the determination of design variables and objective functions, a parametric simulation model was developed. To carry out the parametric simulations, we used a powerful analysis tool, jEPlus (Zhang 2012), which allows users to parameterize fields in an EnergyPlus model and specify a discrete set of values for these fields. jEPlus then parsed the parameter definitions and created a list of cases. Upon execution, it automatically prepared the input files for EnergyPlus according to the job list file, launched EnergyPlus to perform parallel simulations, and finally collected the simulation results (Zhang and Korolija 2010).

Since the total number of combinations of the nine parameters could be very large, requiring a long time to simulate, Latin hypercube sampling (LHS) was used to generate a small, representative sample of a population. For correct sampling of the search space, the sample size taken by the LHS was generally at least ten times the number of input variables, and it was also related to the interaction complexity between input parameters. A 1,000-case sample was simulated, and the results were used to build the relationship between design variables and objective functions by means of the ANN model.

2.3.2 Artificial neural network training and validation

After simulation of all 1,000 cases, the corresponding values of LCC and $LCCO_2$ were obtained according to the definitions in Section 2.2. The major disadvantage of directly using genetic algorithm (GA) or GA-based algorithms for optimization lies in the lower convergence speed to getting an optimal solution (Machairas et al. 2014; Nguyen et al. 2014). The surrogate models are commonly used to replace the computationally original simulation models. The application of surrogate models can be a promising and efficient way to speed convergence by reducing function evaluation cost and/or smoothing noisy response functions. Recently, there have been several surrogate models used in building performance optimization, such as ANNs, response surface methods, data fits, multi-fidelity models, and reduced-order models, Bayesian networks, among which ANNs are the mostly used for good reliability and accuracy (Melo et al. 2014). ANN models use a machine learning method to solve complicated non-linear problems by imitating the complex relationships of biological networks (Caudill and Butler 1993; Li et al. 2019). As it has been proved highly efficient for predicting LCC (Almeida and De Freitas 2016) and $LCCO_2$ (Azari et al. 2016), thus ANN is chosen as the surrogate model to be coupled with NSGA-II in this study.

Based on the input and output data for the 1000 cases, an ANN model was employed to identify the relationship between design variables and objective functions. This study used Neural Network Toolbox in Matlab R2019a to build and train the ANN models. An ANN model is made up of layers of parallel elemental units, called neurons. There are usually three layers: an input layer which receives information, a hidden layer, and an output layer which provides results, as shown in Fig. 5. In the present study, the input layer contained nine neurons corresponding to the nine selected input variables. The output layer was composed of two neurons corresponding to the two objectives. Selecting the

optimal number of neurons for the hidden layer is a critical step in finding the optimal parameters of an ANN model, including weights and biases. If the neurons are underestimated, the ANN's capacity to store information may be reduced. In contrast, an overestimation may induce unnecessary learning for the ANN and even over-fitting. ANN performance is evaluated by means of the regression and the distribution of the relative error between ANN-predicted and EnergyPlus-simulated objectives. A trial-and-error method was used to determine the number of neurons in the hidden layer and the training algorithm, based on an evaluation of the mean squared error (MSE) and the regression coefficients of R between the ANN-predicted and EnergyPlus-simulated objectives, as calculated by Eq. (7) and (8):

$$MSE = \frac{1}{n} \bullet \sum_{i=1}^{n} (y_i - \hat{y}_i) \tag{7}$$

$$R = \sqrt{1 - \frac{\sum_{i=1}^{n} (y_i - \hat{y}_i)^2}{\sum_{i=1}^{n} (y_i - \bar{y}_i)^2}} \tag{8}$$

where y_i are all the data predicted by the ANN model, and $\bar{y}_i$ is the mean value of y_i. In the trial-and-error process, we randomly selected 70% of the data to train the ANN and optimize weights and biases, while the remaining 30% of the data was used for validation and testing.

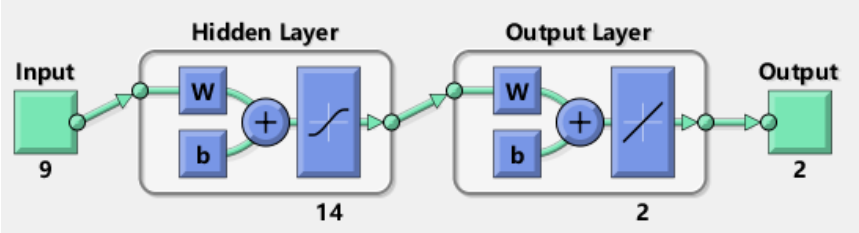

Fig. 5. Structure of the ANN model

Fig. 6 depicts the relationship between the number of neurons in the hidden layer, and the MSE and R between predicted and simulated objectives. It can be seen that the MSE decreased with the increase in the number of neurons in the hidden layer, while the R increased. When the number of neurons reached 14, the regression coefficient of R was higher than 0.98, demonstrating very sound agreement between the predictions and the simulations. At this point, a further increasing in the number of neurons in the hidden layer would not significantly improve the R, but it would increase the training time. To balance the training time with the model complexity, therefore, this study used 14 neurons in the hidden layer of the ANN model. The MSE for the ANN model with 14 neurons in the hidden layer was 14, which was small enough for good performance by the ANN prediction.

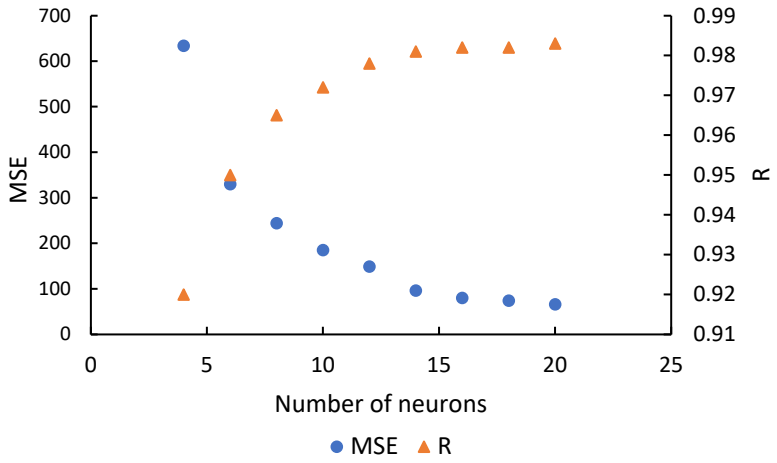

Fig. 6. Relationship between number of neurons in the hidden layer, and the MSE and R between predicted and simulated objectives

Three popular algorithms are available for ANN prediction, as shown in Table 7. The best prediction would be provided by the algorithm that achieved the smallest MSE and largest R. Our testing identified the Bayesian regularization algorithm as the best option, and therefore we used this algorithm for ANN model training.

Table 7 MSE and R of three training algorithms

Training algorithm	MSE	R
Levenberg-Marquardt	27	0.98
Bayesian regularization	14	0.981
Scaled conjugate gradient	120	0.975

2.3.3 Multi-objective optimization

After the ANN model had been trained and validated, it was used as the evaluation function for LCC and $LCCO_2$ estimations within the multi-objective algorithm. For a multi-objective problem, there was no unique optimal solution that could be identified as the best for all the objectives simultaneously. Instead, a Pareto-optimal set of trade-off optimal solutions was obtained, to guide decision makers. The NSGA-II is an evolution algorithm characterized by higher computation efficiency, greater probability of creating good solutions, and maintenance of population diversity by means of the crowding comparison (Deb et al. 2001). Therefore, the NSGA-II was chosen for the optimization in this study.

Like any other GA, NSGA-II is based on the evolution of a population of "individuals", each of which is a solution to the optimization problem. In this study, an individual is a design option to be implemented on a building. To simulate the evolution process, each design variable (x_1, x_2, … x_n) represents a gene, and a combination of design variables $\{x_1, x_2, \ldots x_n\}^T$ constitute a chromosome. An individual is represented by the chromosome, as shown in Fig. 7. NSGA-II determines the iterative evolution of a population of individuals, by means of a process of inheritance, selection, crossover and mutation. Elite strategy is further applied to search for the excellent individuals.

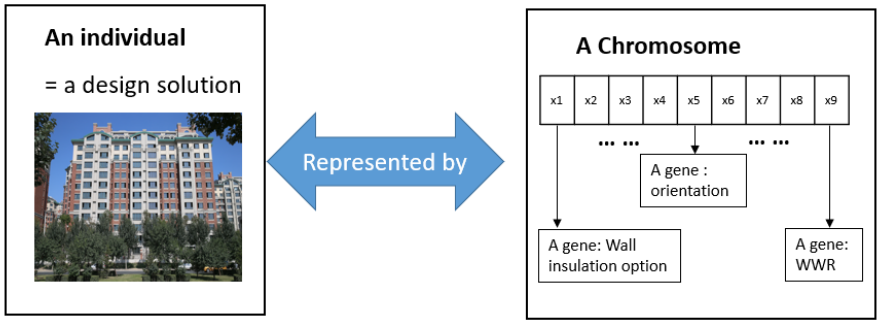

Fig. 7. A solution to the design optimization problem, represented by a chromosome.

The optimization process is illustrated in Fig. 8. First, the initial population of individuals was generated arbitrarily by evolutionary algorithms. The developed ANN model was used as a fitness function to evaluate the performance of LCC and $LCCO_2$ ($\underline{F(\mathbf{x})}$) for those individuals ($\underline{\mathbf{x}}$). The assessment results served as feedback to the evolutionary algorithm, in which individuals yielding lower $\underline{F(\mathbf{x})}$ were more desirable. The random selection, crossover, and mutation operation generated individuals that were more suitable for the environment. The population continued to reproduce and evolved to increasingly better generations. The evolution stopped when at least one of the following criteria was met: a maximum number of generations was achieved, and the average relative change between two successive generations was lower than a tolerance value. Finally, a set of Pareto-optimal solutions was generated. The optimal design scheme can be selected from the Pareto-optimal solutions according to the preferences of the designers.

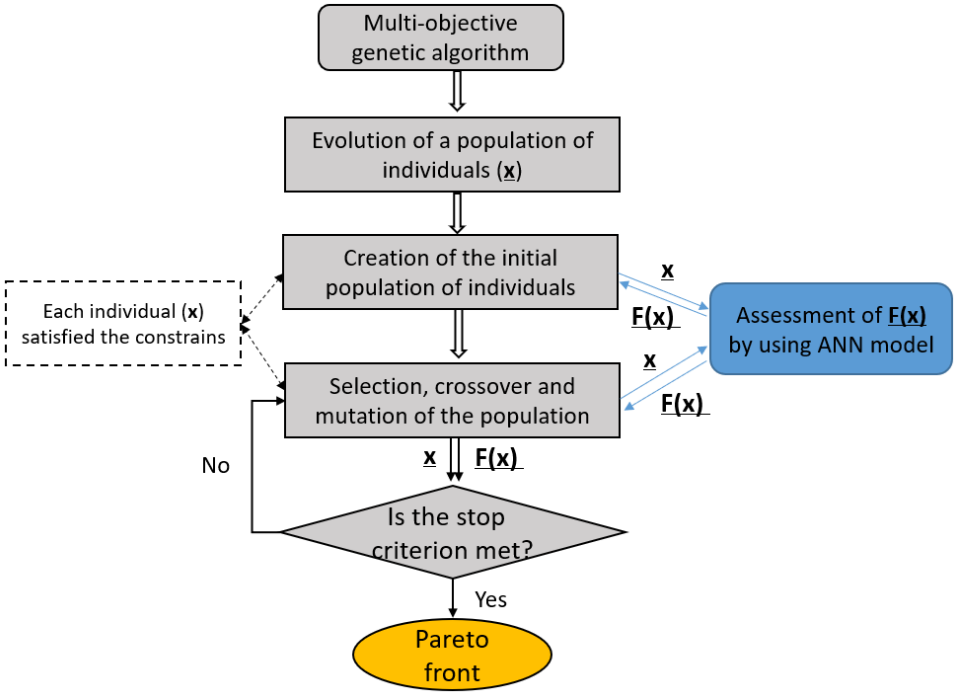

Fig. 8. Flowchart of the NSGA-II optimization with ANN model

To set up an optimization process, the parameters should be defined. They include population size, number of generations, and crossover and mutation probability. Determination of the values for these parameters usually depends on the grade of nonlinearity of the optimization problem, the types of input variables (continuous or discrete), and the dimension of the problem space (Deb 2001). In general, it is recommended that the population size be two to six times the number of input variables (Ascione et al.

2016), usually within the range of 10 to 200 (Lei et al. 2005). The crossover probability controls the dominant crossover operator in the process of optimization. A larger value of crossover probability may damage the increase of excellent individuals, while a lower value leading to slow evolution, yields a range of 0.4~0.99 (Lei et al. 2005). Mutation refers to small, random variation in the genotype (Weise 2009). The mutation probability controls the frequency of the mutation operation, with a recommended value range of 0.0001–0.1 (Lei et al. 2005). On the basis of the literature analysis and as a trade-off with the available computational capacity, the following parameters were set in NSGA-II: population size = 200, maximum number of generations = 100, function tolerance = 0.0001, crossover probability = 0.9, and mutation probability = 0.1.

3. Results

This section first compares the heating and cooling loads in a CB and in the initial design of the PB. The results of the optimization methodology are then presented.

3.1 Comparison of energy demand in passive and conventional buildings

With dynamic simulation, it is possible to compare the heating and cooling loads between a CB and the initial design of the PB with and without NV, and thus to calculate the energy-saving potential with NV. As shown in Fig. 9, the annual heating load in the PB was reduced significantly, by about 75%, compared with that in the CB, while the annual cooling load increased by about 40%. This increase occurred because the additional insulation, high-performance windows and high airtightness prevented the passive house from releasing heat indoors. Therefore, internal energy gains, including residents' activity and metabolism as well as solar heat gains, would unavoidably lead to increased cooling demand. If no NV was used during the summer season, the cooling loads would be 15.13 kWh/(m^2·a) in the CB and 21.21 kWh/(m^2·a) in the PB. The use of the HV strategy (described in Section 2.1.2) reduced the cooling load to 0.99 kWh/(m^2·a) in the CB and 4.71 kWh/(m^2·a) in the PB. It is worth mentioning that for the CB, the cooling energy would be negligibly small in comparison with the 50.18 kWh/(m^2·a) required for heating. Proper use of NV can provide very good thermal comfort in the summer. However, the PB has a cooling energy demand that is comparable to that for heating. In addition, the cooling energy cost is usually three times higher than the cost of heating. Therefore, cooling plays a more important role in the overall energy demand of the PB, even in a heating-dominated region. A similar phenomenon was reported in previous studies (Mlakar and Štrancar 2011; Masoud et al. 2015; Psomasa et al. 2016). To save energy in the Harbin household sector, the use of NV is proposed as a passive method of cooling. In existing buildings, the residents would be the driver in optimizing the natural airflow indoors, whereas for projected buildings, the building design is the main factor to be taken into account.

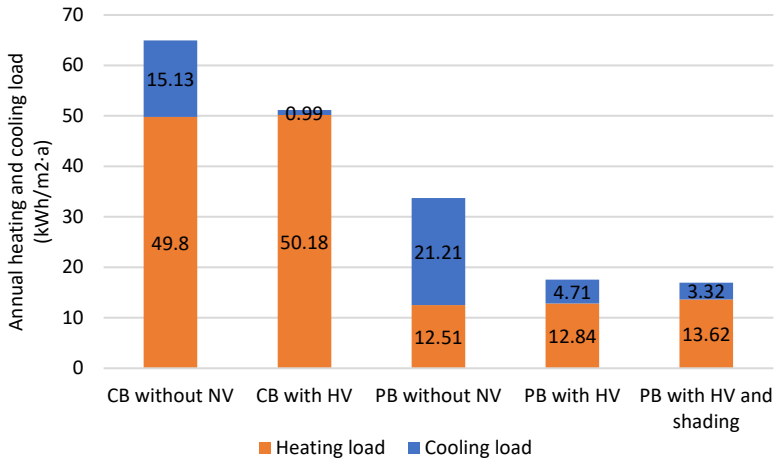

Fig. 9. Comparison of energy demand in passive and conventional buildings. Note: 'NV' refers to natural ventilation, and 'HV' to hybrid ventilation.

The cases above aimed only to study the effect of NV without a shading device. We also studied the effect of an external shading device on cooling energy saving potential and the opposing increase in heating demand. The shading system adopts overhangs above the south-facing windows. We used a depth of 0.8 m for analysis. As shown in Fig. 9, when the PB was equipped with horizontal overhangs on the south windows, the cooling load decreased further, by 1.39 kWh/(m^2·a), with a slight increase of 0.78 kWh/(m^2·a) in heating load. This difference arose from the different solar altitudes in winter and summer. In summer, the solar radiation is strong, and the solar altitude is high; thus, horizontal overhangs would block the solar heat effectively and reduce the cooling load. However, in winter, solar radiance decreases, and the solar altitude is much lower, so that most areas of windows are exposed to the sunlight, even with overhangs, leading to a smaller impact. Therefore, external shading by an overhang is preferred in Harbin. Since shading depth also affects the daylight illuminance and lighting energy use, the optimal depth needs to be parametrically determined.

3.2 Multi-objective optimization of LCC and LCCO_2 emissions

This study aimed to simultaneously minimize the cost and CO_2 emissions over the life cycle of the building by means of the multi-objective optimization algorithm NSGA-II. After 249 iterations, the average change in the spread of Pareto solutions was small, and the optimization results converged. The optimization process generated 70 solutions that formed a Pareto front. Fig. 10 displays the costs and CO_2 emissions for the 1000 database cases, the PB, the CB, and the Pareto-front cases. Each point in the figure is a solution associated with a set of decision variables representing a design scenario. The Pareto-front solutions yielded better building performance as far as the two optimization objectives are concerned. For the initial design of the PB, the LCC and LCCO_2 emissions were 1320 CNY/m^2 and 596 kg/m^2, respectively, and both were much lower than the CB, as depicted by the blue and orange dots in Fig. 10. These results indicate that energy use had a dominant effect on the building life cycle. Comparison of the Pareto-front solutions with the initial design of the PB reveals the significant improvement of the two objectives after optimization. The LCC and the LCCO_2 emissions were

reduced by 10.9–18.9% and 13.5–22.4%, respectively.

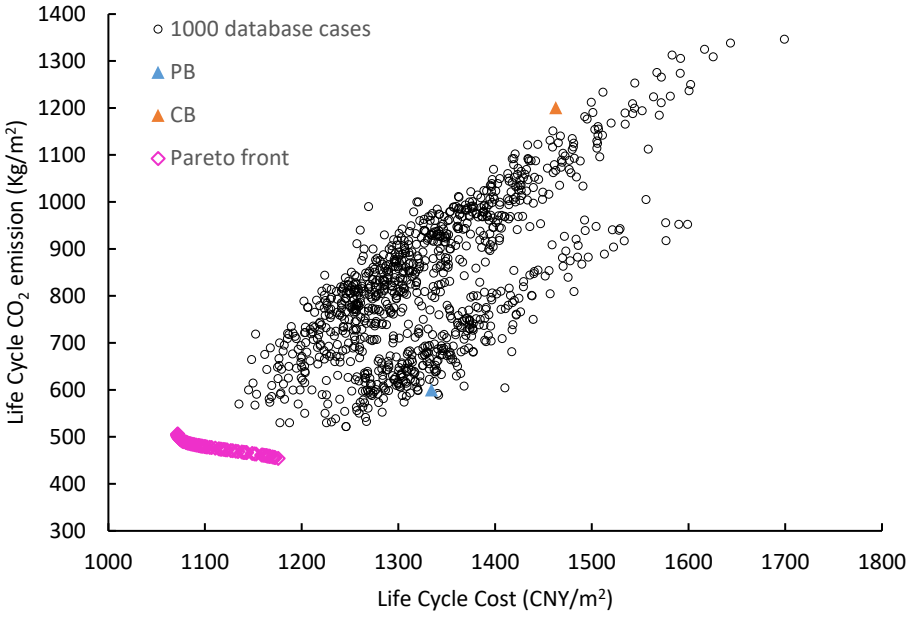

Fig. 10 Costs and CO_2 emissions for the 1000 database cases, the PB, the CB and the Pareto-front solutions

Primary energy consumption, one of the most important indicators of building energy efficiency, combines heating, cooling and electricity energy consumption. For severe cold climate regions, the Chinese PH standard requires the annual primary energy consumption to be lower than 60 KWh/(m^2·a) (MOHURD 2019). In the present study, the primary energy consumption for the initial design of the PB was 50.8 KWh/(m^2·a). The Pareto-front solutions were within the range of 41.3–47.6 KWh/(m^2·a). All the Pareto solutions met the PH standard and were lower than in the initial design. Thus, the optimal solutions from the perspective of life cycle costs and carbon emissions also exhibit better energy performance. If the model had included HVAC system parameters, it would have been possible to further reduce the final cost because the systems would have been downsized as the load declined.

3.3 Design variables of the optimal solutions

Three typical solutions were selected from the Pareto front for detailed analysis, depicted in Fig. 11. As can be observed, the two objective functions conflicted with each other within the Pareto-front solutions. The smaller value of the objective represents the better behavior. For example, point A had high CO_2 emissions but low cost, and represents an optimal case for the minimization of LCC. Point C was the optimal case for minimization of $LCCO_2$ emissions. Point B had intermediate values for both criteria. Moving from point B to point A, the figure shows that with a slight increase in LCC, a considerable reduction in $LCCO_2$ emissions was achieved.

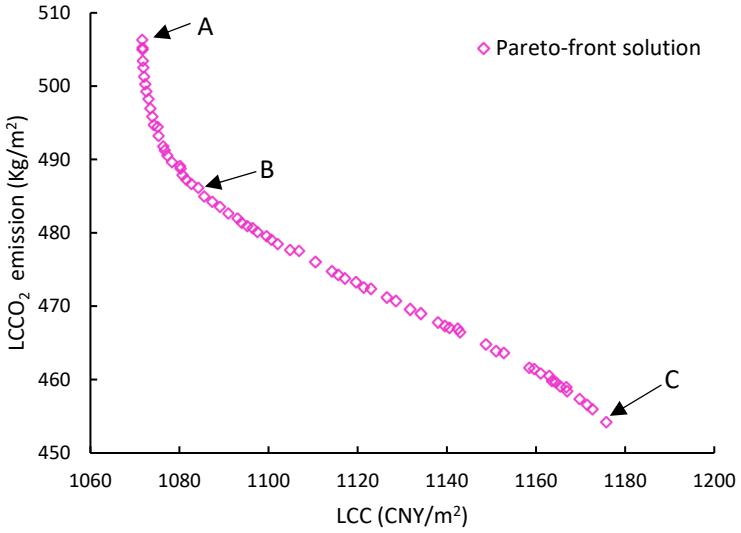

Fig. 11. The Pareto-front solutions for LCC and $LCCO_2$ emissions.

The design variables for the Pareto-front solutions A, B, and C and the initial design of the PB are specified in Table 8. Some of the parameters are the same or similar among the solutions, while other parameters differ.

Table 8 Design variables for the Pareto-front solutions and the initial design of the PB

Decision variables	Initial design	Pareto solution A	Pareto solution B	Pareto solution C	Pareto solutions	
					Min Value	Max values
x1-Wall insulation thickness (mm)	300	260	265	266	255	266
x2-Roof insulation thickness (mm)	300	330	330	330	330	330
x3-South overhang depth (m)	0	0.9	0.6	0.4	0.2	0.9
x4-Window type	Type 6	Type 4	Type 4	Type 6	Type 4	Type 6
x5-Orientation (°)	45	4.6	4	3.02	-5	8
x6-WWR N (%)	28.53	20.13	17	14.7	15	22
x7-WWR E (%)	5.71	6	5	5	5	6
x8-WWR S (%)	33.93	36.20	27.1	33.4	25	36
x9-WWR W (%)	4.16	5.05	5	5	5	5.05
LCC (CNY/m^2)	1320	1072	1087	1176	1072	1176
$LCCO_2$ emissions (Kg/m^2)	585	506	484	454	454	506

For the external wall insulation thickness, the most highly recommended values for Pareto-front solutions A, B, and C were very similar; these values are 260 mm (U = 0.124), 265 mm (U = 0.122) and 266 mm (U = 0.121), respectively. Compared to the initial design of 300 mm (U = 0.1), the optimal design solutions had smaller thicknesses. Thicker thermal insulation can improve the thermal performance of a building envelope and effectively reduce the heating energy consumption of the building; however, it can increase the investment cost and the usage of insulation materials. An increase

in insulation thickness reportedly corresponds to higher material cost, while the energy savings is large at first but soon disappears (Carreras et al. 2015). When the LCC is considered rather than the energy cost, a thicker insulation will no longer be economically beneficial. This approach can also be used for analysis of the minimum CO_2 emissions solution, with the cost replaced by the environmental burdens arising from insulation materials and energy consumption. The same analysis applies to roof insulation. Note that, because the roof is constructed differently from the external wall, the determined thicknesses were 330 mm (U = 0.109) for Pareto-front solutions A, B, and C. The similarities of the three solutions in regard to external envelope insulation meant that there was little variation among the results for the two criteria.

Among the six window glazing types, all the solutions converged toward the triple low-e types. This result was due mainly to their high thermal performance. However, type 4 (U = 1.2, SHGC = 0.55) was obtained for Pareto-front solutions A and B, and type 6 (U = 0.8, SHGC = 0.5) for Pareto-front solution C. The reason for these different types might have been the different LCC and $LCCO_2$ achieved. As shown in Table 4, there was a price difference of 700 CNY/m^2 between type 4 and type 6, indicating that a slight improvement in the window thermal performance would be achieved at a high cost. The higher initial cost for the window means that it would not translate into a significant decrease in LCC, making type 6 financially unfeasible. Meanwhile, Pareto-front solution C minimized $LCCO_2$. If the priority was to reduce $LCCO_2$, a fairly low window U value would be preferred for reducing the annual heating energy consumption.

The results in Table 8 show that the major building façades of the non-dominant designs were oriented toward the south, with a range from -5° to 8°, and were mainly distributed in the range of 0-6° from south to east, which is consistent with a previous study conducted in Harbin (Han et al. 2017). The optimized orientation was different from the original design (45° from south to east). The primary reason for this different design orientation may be the consideration of prevailing wind direction. The present study used prevailing wind directions in Harbin based on the typical meteorological year (TMY) weather data, which are south and southwest. In the original building design, the prevailing wind direction of the local microclimate was used, which is southeast. Therefore, in the optimized design, a south orientation is beneficial to NV in summer and reduces heating energy consumption in winter with regard to the Pareto solutions, while a southeast orientation is beneficial to NV in the original design.

The ratios of glazing on the building façade have significant effects on heating and cooling energy consumption and the indoor visual, which interact considerably with each other. There were larger ranges of WWRs in south and north façades than in west and north façades. The optimal WWRs on the west and east were very close to their lower limits of 5%. This is commonly understood in cold climates because even windows with triple layers have much higher U-value and are considered to be more expensive than an insulated external wall. Larger windows increase heating and cooling energy use, which will not be compensated for by decreased electric lighting (Marino et al. 2017). Additionally, west-facing windows receive too much heat from solar radiance in summer, which increases the cooling energy consumption, while the windows contribute less solar heat gain in winter (Zhai et al. 2019). Furthermore, as mentioned above, the prevailing wind directions were south and southwest, so that west- and east-facing windows contribute little to NV. Therefore, low WWRs on the west and east

façades would be preferable. The largest WWRs were observed on the south façade, with a range of 25–36% for the Pareto-front solutions. A large south window would benefit from solar heat gains in winter, and would not receive too much heat from solar radiation in summer because of the shading overhang. The obtained optimal window size for each solution also took into account the daylight and NV. The optimal north WWRs were lower than those on the south, and the distribution was relatively narrow, with a range of 15–22%. Since the solar radiation is the lowest on the north side of a building, a larger window on the north façade would increase the heating load. However, the subject of this study was a typical high-rise residential building with large wall area on the north and south sides. The main rooms were oriented to the north and south. An increase in WWR would allow more daylight to enter a room. Larger windows on the north façade with small windows on the east or west would improve the indoor daylight in a specific room. Moreover, the north windows could provide cross ventilation when coupled with south windows. Therefore, it can be concluded that the north window enhanced NV and reduced lighting electricity, despite the increase in heating energy. In addition, the lower total WWRs occurred in the solutions with the highest-performance window type, resulting in better economic performance. For example, solution A had a larger window than solution C because the former solution used a cheaper window.

Regarding the characteristics of the overhang depth, the optimization yielded a wide diversity among the solutions, with a distribution of 0.2–0.9 m, as shown in Table 8. Shading elements can be crucial for reducing the cooling load in summer, while conversely raising energy consumption for heating in winter as well as lighting. In addition, determination of the overhang depth depends on the window size. If a small window on the south is optimized with a Pareto-front solution, the corresponding overhang depth is fairly small.

To evaluate the impact of each variable on each objective quantitatively within the Pareto-optimal solutions, the standard rank regression coefficient (SRRC) and partial rank correlation coefficient (PRCC) were calculated as indicators. The SRRCs measure the linear impacts of design parameters, while the PRCCs provide a sensitivity analysis that excludes the correlation impacts between the design parameters. Since the variables had different units and relative magnitudes, the original data was normalized by ranking. A regression analysis was then performed on the transformed data. Fig. 12 illustrates the SRRC and PRCC for each variable and objective. The sensitivity rankings of the two indicators were the same with different sensitivity measures. The PRCCs were obviously larger than the SRRCs, which indicates the existence of non-linear impacts. Positive SRRCs and PRCCs signify a positive correlation, and vice versa. The results show that the variables of roof insulation thickness, orientation, and WWR in the east and west façades had almost no effect on either of the two objectives, and the wall insulation thickness had little impacts. Thus, the optimized ranges of these variables favored both objectives. Decision-makers can select any values within the optimized ranges for these variables. The other variables, including south overhang depth, window type, and north and south WWRs, had various impacts on the two objectives. The coefficients of south and north WWR were clearly positive for LCC, while negative for $LCCO_2$ emissions. In the solution favoring the minimization of LCC, window type was responsible for the largest part, and the lower limit within the optimized range is recommended as a negative coefficient concerned. For the minimization of $LCCO_2$ emissions, the upper limit is recommended. The depth of the south overhang also had opposite effects

on LCC and $LCCO_2$ emissions. A larger overhang depth within the optimized range would be preferable for reducing LCC, but a somewhat smaller depth is indicated for reducing $LCCO_2$ emissions.

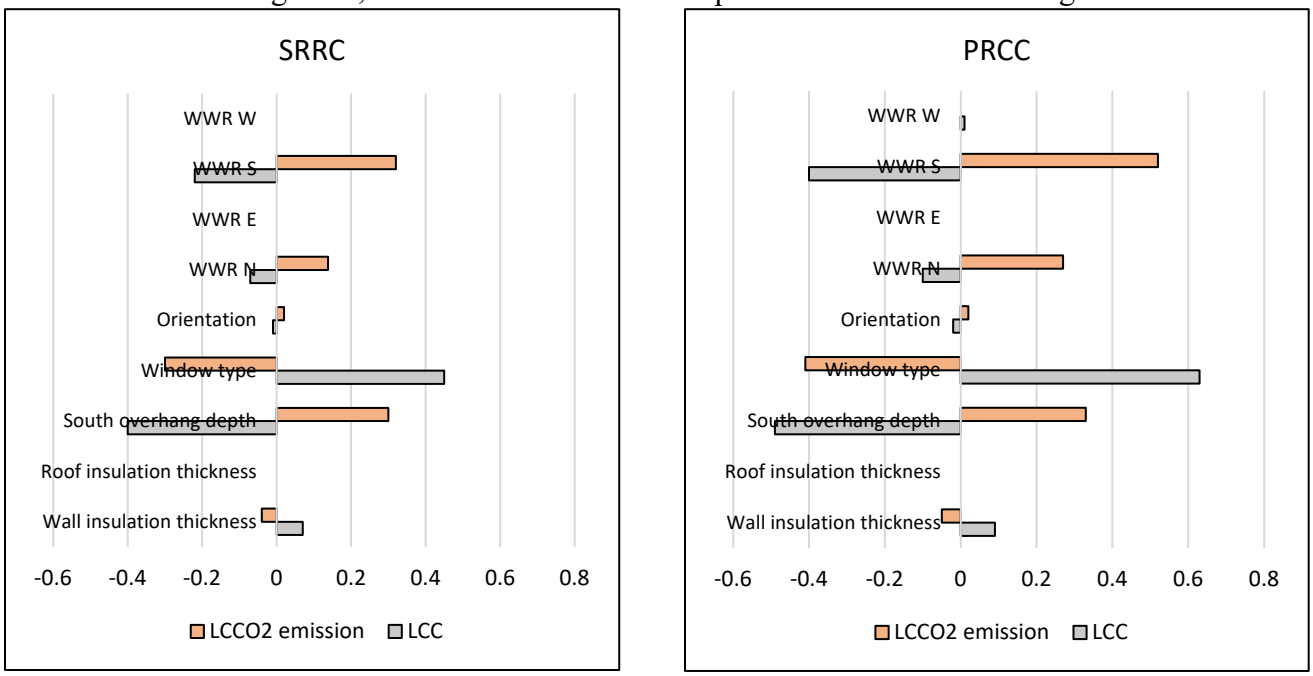

(a) (b)

Fig. 12. Regression/correlation coefficients of all variables using two regression methods: (a) standard rank regression coefficients and (b) partial rank correlation coefficients.

4. Discussion

The design variables affected the two objective functions interactively. In a local analysis by Marino et al. (2017), the most economical value of WWR was influenced by the envelope thermal insulation. Zhai et al. (2019) found that different combinations of external shading and window type had various effects on heating, cooling and lighting energy consumption as well as thermal comfort. The studies revealed the importance of global design optimization for architects in identifying the best parameter combinations. For improvement of more than one objective simultaneously, multi-objective optimization is beneficial.

In this study, the two selected objectives were not completely independent because the costs and emissions linked to energy usage dominate LCC and $LCCO_2$ emissions, respectively. This indicates that design solutions with low energy demand would favor both objectives in most cases. However, for Pareto solutions on the leading edge, the two objectives conflict with each other. In this study, electricity was assumed for summer cooling and coal for winter heating, as these are the traditionally used energy sources in Harbin. As calculated, unit energy prices of coal and electricity are 0.0863 CNY/kWh and 0.277 CNY/kWh, respectively. With the same amount of energy consumed, the cost of cooling is 3.2 times higher than the cost of heating. However, unit CO_2 emission for coal (0.654 kg/kWh) is higher than that for electricity (0.532 kg/kWh). This leads to a variety of building design solutions in response to economic and environmental concerns. A solution with lower demand for cooling than for heating is likely to exhibit better economic performance. The two objective functions

would allow optimization on energy costs and emissions for the different energy-source combinations.

The method adopted in this study could be employed for other building types and climates; however, the results are somewhat specific to the reference building because financial and emissions parameters were held constant, and costs and emissions factors were case-specific. Changes in financial parameters such as mortgage rate and discount rate would directly affect the steepness of the resultant Pareto front (Tokarik and Richman 2016). Therefore, the sensitivity of the optimized results to specific parameters should be evaluated in the future.

Besides the costs and emissions addressed in this study, the building design may be influenced by individualized factors such as architectural aesthetics and overall vision, in addition to factors associated with social impact. For example, the thickness of wall insulation will directly affect the use area of the building. However, it is hard to consider all these factors quantitatively. This study was conducted from the viewpoint of sustainable development, and the results based on two-objective optimization are plausible.

5. Conclusion

In this study, we constructed a building energy model with hybrid ventilation and light-dimming control in EnergyPlus. We then used the multi-objective optimization algorithm NSGA-II to find optimal building envelope design solutions that minimized the life cycle costs and emissions. A series of Pareto optimal solutions were identified. The main conclusions are as follows:

(1) In a severe cold region, the annual heating load in passive buildings was reduced by about 75% from that in conventional buildings, while the cooling load increased by 40%. With the designed natural ventilation in summer, the cooling load for the reference PB decreased from 21.21 kWh/(m^2·a) to 4.71 kWh/(m^2·a). Therefore, NV should be fully considered before conducting the design optimization.

(2) The optimization generated a total of 70 Pareto optimal solutions that significantly improved the two objectives. Compared with the initial design of the reference building, the LCC and LCCO_2 emissions were reduced by 10.9–18.9% and 13.5–22.4%, respectively.

(3) Among Pareto optimal solutions, the roof insulation was optimized to a thickness of 330 mm. The optimized wall insulation thickness was 255–266 mm less than the 300 mm of the original design. To increase the current passive-level insulation of walls was not found to be cost-effective. All the solutions converged toward triple low-e glazing window types. Building orientation almost converged to the south with a range of 0° to 6° from south to east. The external shading had a positive effect on the objectives in all the solutions. As for WWRs, the west and east façades had the lowest values, close to their lower limits of 5%. The largest WWRs were found on the south façade, with a range of 25–36%. WWRs on the north façade were within the range of 15–22%.

Acknowledgment

This work was supported by the National Natural Science Foundation of China (No. 51938003, 51678179).

References

Almeida RMSF, De Freitas VP (2016). An insulation thickness optimization methodology for school buildings rehabilitation combining artificial neural networks and life cycle cost. *Journal of Civil Engineering and Management*, 22: 94-103.

Alsayeda MF, Tayeh RA (2019). Life cycle cost analysis for determining optimal insulation thickness in Palestinian buildings. *Journal of Building Engineering*, 22: 101-112.

Ameur M, Kharbouch Y, Mimet A (2020). Optimization of passive design features for a naturally ventilated residential building according to the bioclimatic architecture concept and considering the northern Morocco climate. *Building Simulation*, 13: 677–689.

Ascione F, Bianco N, De Stasio C, Mauro GM, Vanoli GP (2016). Multi-stage and multi-objective optimization for energy retrofitting a developed hospital reference. *Applied Energy*, 174: 37-68.

ASHRAE (2017). Standard 55-2017. Thermal environmental conditions for human occupancy.

Azari R, Garshasbi S, Amini P, Rashed-Ali H, Mohammadi Y (2016). Multi-objective optimization of building envelope design for life cycle environmental performance. *Energy and Buildings*, 126: 524-534.

Baba FM, Ge H (2020). Overheating risk of a single-family detached house built at different ages under current and future climate in Canada. *E3S Web of Conferenc*es, 172: 02004.

Bichiou Y, Krarti M (2011). Optimization of envelope and HVAC systems selection for residential buildings. *Energy and Buildings*, 43: 3373-3382.

Boermans T, Bettgenhäuser K, Hermelink A (2011). Cost optimal building performance requirements, European Council for an Energy Efficient Economy.

BS EN 15459-1 (2017). Energy performance of buildings. Economic evaluation procedure for energy systems in buildings.

BS EN 15978 (2011). Sustainability of construction works. Assessment of environmental performance of buildings. Calculation method.

Building Energy Research Center (2016). Tsinghua University. China Building Energy Use 2016. China Architecture & Building Press. (in Chinese).

Cabeza LF, Barreneche C, Miró L, Morera JM, Bartolí E, Inés Fernández A (2013). Low carbon and low embodied energy materials in buildings: A review. *Renewable & Sustainable Energy Reviews*, 23: 536–42.

Carreras J, Boer D, Cabeza LF, Medrano M, Jiménez L, Guillén-Gosálbez G (2017). Reducing the life cycle environmental impact of buildings following a simulation-optimization approach. *Advances in Energy Systems Engineering*, 823-39.

Carreras J, Boer D, Guillén-Gosálbez G, Cabeza LF, Medrano M, Jiménez L (2015). Multi-objective optimization of thermal modelled cubicles considering the total cost and life cycle environmental impact. *Energy and Buildings*, 88: 335–46.

Carreras J, Pozo C, Boer D, Guillén-Gosálbez G, Caballero JA, Ruiz-Femenia R, Jiménezc L (2016). Systematic approach for the life cycle multi-objective optimization of buildings combining

objective reduction and surrogate modeling. *Energy and Buildings*, 130: 506-518.
Caudill M, Butler C (1993). Understanding Neural Networks: Computer Explorations—Volume 1 Basic Networks, The MIT Press, Cambridge, MA.
de Dear RJ, Brager GS (2002). Thermal comfort in naturally ventilated buildings: Revisions to ASHRAE Standard 55. *Energy and Buildings*, 34: 549-61.
Deb K (2001). Multi-objective Optimization Using Evolutionary Algorithms. John Wiley & Sons.
Deb K, Pratap A, Agarwal S, Meyarivan T (2002). A fast and elitist multiobjective genetic algorithm: NSGA II. *IEEE Transactions on Evolutionary Computation*, 6: 182-197.
Delgarm N, Sajadi B, Delgarm S (2016). Multi-objective optimization of building energy performance and indoor thermal comfort: A new method using artificial bee colony (ABC). *Energy and Buildings*, 131: 42-53.
Dylewski R, Adamczyk J (2016). The environmental impacts of thermal insulation of buildings including the categories of damage: A Polish case study. *Journal of Cleaner Production*, 137: 878–87.
EU Commission (2012). Commission Delegated Regulation (EU) No 244/2012 of 16 January 2012 supplementing Directive 2010/31/EU of the European Parliament and of the Council on the energy performance of buildings.
Ferrara M, Sirombo E, Fabrizio E (2018). Automated optimization for the integrated design process: The energy, thermal and visual comfort nexus. *Energy and Buildings*, 168: 413-427.
Garshasbi S, Kurnitski J, Mohammadi Y (2016). A hybrid Genetic Algorithm and Monte Carlo simulation approach to predict hourly energy consumption and generation by a cluster of Net Zero Energy Buildings. *Applied Energy*, 179: 626-37.
Global ABC (2020). Global status report for buildings and construction. Global Alliance for Buildings and Construction.
Guo H, Huang L, Song W, Wang X, Wang H, Zhao X (2020). Evaluation of the Summer Overheating Phenomenon in Reinforced Concrete and Cross Laminated Timber Residential Buildings in the Cold and Severe Cold Regions of China. *Energies*, 13(23): 6305.
Guo S, Yan D, Hu S, Zhang Y (2021). Modelling building energy consumption in China under different future scenarios. *Energy*, 214: 119063.
Hajare A, Elwakil E (2020). Integration of life cycle cost analysis and energy simulation for building energy-efficient strategies assessment. *Sustainable Cities and Society*, 61: 102293.
Han Y, Yu H, Sun C (2017). Simulation-based multiobjective optimization of timber-glass residential buildings in severe cold regions. *Sustainability*, 9(12): 2353.
ISO 21930 (2017). Sustainability in buildings and civil engineering works - Core rules for environmental product declarations of construction products and services
Jafari A, Valentin V (2018). Selection of optimization objectives for decision-making in building energy retrofits. *Building and Environment*, 130: 94-103.
Kiss B, Sazlay Z (2020). Modular approach to multi-objective environmental optimization of buildings. *Automation in Construction*, 111:103044.
Lei YJ, Zhang SW, Li XB, Zhou CM (2005). MATLAB Genetic Algorithm Toolbox and Application, Xidian University Press. (in Chinese).
Li DHW, Yang L, Lam JC (2013). Zero energy buildings and sustainable development implications - A review. *Energy*, 54: 1-10.

Li Z, Dai J, Chen H, Lin B (2019). An ANN-based fast building energy consumption prediction method for complex architectural form at the early design stage. *Building Simulation*, 12: 665–681.

Lu S, Wang R, Zheng S (2017). Passive optimization design based on particle swarm optimization in rural buildings of the hot summer and warm winter zone of China. *Sustainability*, 9 (12).

Machairas V, Tsangrassoulis A, Axarli K (2014). Algorithms for optimization of building design: A review. *Renewable and Sustainable Energy Reviews*, 31: 101-112.

Marino C, Nucara A, Pietrafesa M (2017). Does window-to-wall ratio have a significant effect on the energy consumption of buildings? A parametric analysis in Italian climate conditions. *Journal of Building Engineering*, 13: 169-183.

Mateus R, Silva SM, Almeida MGD (2019). Environmental and cost life cycle analysis of the impact of using solar systems in energy renovation of southern European single-family buildings. *Renewable Energy*, 137: 82-92.

Melo AP, Cóstola D, Lamberts R, Hensen JLM (2014). Development of surrogate models using artificial neural network for building shell energy labelling. *Energy Policy*, 69: 457–466.

MOHURD (2010). Design standard for energy efficiency of residential buildings in severe cold and cold zones (JGJ 26-2010). Ministry of housing and Urban-Rural Development of China. (in Chinese).

MOHURD (2019). Technical Standards for Near-Zero Energy Buildings (GB/T 51350-2019). Ministry of housing and Urban-Rural Development of China. (in Chinese).

Nguyen A, Reiter S, Rigo P (2014). A review on simulation-based optimization methods applied to building performance analysis. *Applied Energy*, 113: 1043-1058.

Płoszaj-Mazurek M, Rynska E, Grochulska-Salak, M (2020). Methods to optimize carbon footprint of buildings in regenerative architectural design with the use of machine learning, convolutional neural network, and parametric design. *Energies*, 13(20), 5289.

Sartori I, Hestnes AG (2007). Energy use in the life cycle of conventional and low-energy buildings: A review article, *Energy and Buildings*, 39: 249-57.

Spentzou E, Cook MJ, Emmitt S (2018). Natural ventilation strategies for indoor thermal comfort in Mediterranean apartments. *Building Simulation*, 11: 175–191.

Thalfeldt M, Pikas E, Kurnitski J, Voll H (2013). Facade design principles for nearly zero energy buildings in a cold climate. *Energy and Buildings*, 67: 309-321.

Tokarik MS, Richman RC (2016). Life cycle cost optimization of passive energy efficiency improvements in a Toronto house. *Energy and Buildings*, 118: 160-169.

Wang R, Lu S, Feng W, Xu B (2020). Tradeoff between heating energy demand in winter and indoor overheating risk in summer constrained by building standards. *Building Simulation*.

Weise T (2009). Global optimization algorithms – Theory and application, http://www.itweise.de.

Yang X, Zhang S, Xu W (2019). Impact of zero energy buildings on medium-to-long term building energy consumption in China. *Energy Policy*, 129: 574-586.

Zhai Y, Wang Y, Huang Y, Meng X (2019). A multi-objective optimization methodology for window design considering energy consumption, thermal environment and visual performance. *Renewable Energy*, 134: 1190-1199.

Zhang Y, Korolija I (2010). Performing complex parametric simulations with jEPlus. Paper presented at the 9th International Conference on Sustainable Energy Technologies, Shanghai.

Zhao M, Künzel HM, Antretter F (2015). Parameters influencing the energy performance of residential buildings in different Chinese climate zones. *Energy and Buildings*, 96: 64-75.